Yokohama, Japan, May 30–June 4, 2004
Paper No. 104

Interactions between Free-surface, Free-stream Turbulence and Cavity Recirculation in Open Channel Flows: Measurements and Turbulence Manipulation

Hubert Chanson[1], Carlos A. Gonzalez[2]

1: Department of Civil Engineering, The University of Queensland, Brisbane Qld 4072, Australia, h.chanson@uq.edu.au
2:Department of Civil Engineering, The University of Queensland, Brisbane Qld 4072, Australia, c.gonzalez@uq.edu.au

Abstract New experiments were conducted in a large stepped channel with a 22º slope operating at large Reynolds numbers. Interactions between free-surface and cavity recirculation were systematically investigated in the skimming flow regime. Turbulence manipulation was further conducted and identical experiments were performed with 4 configurations. Basic results demonstrated a strong influence of cavity vanes (longitudinal ribs) on the air-water flow properties in both free-stream and cavity flows. The air-water flow structure (bubble and droplet size distributions, clustering factor) was significantly affected by the presence of vanes, and greater spray production was observed with the vanes. Air-water velocity and turbulence distributions highlighted further a major impact of the vanes on the entire flow.

1. Introduction

The interactions between flowing waters and atmosphere may lead to strong air-water mixing and complex multiphase flow situations. Air-water flows have been studied only recently. Since the 1960s, numerous researchers studied gas entrainment in liquid flows, focusing on low void fractions (C < 5%). Few research projects have been engaged in strongly-turbulent flows associated with strong free-surface aeration (Wood 1991, Chanson 1997). One extreme flow situation is a supercritical flow down a stepped invert. This chute design is common for overflow spillways of gravity and embankment dams (Chanson 2001). Although most modern structures were designed with flat horizontal steps, recent studies hinted means to enhance the rate of energy dissipation (see below).
In the present study, new experiments were conducted in a large stepped channel with a 22º slope. Interactions between free-surface and cavity recirculation, as well as turbulence manipulation were systematically investigated in the skimming flow regime. The results provide a new understanding of the complicated air-water structure.

Bibliographic review

During the 19th century, overflow stepped spillways were selected frequently with nearly one third ofe dams built in USA being equipped with a stepped cascade. More recently, the 1980s and 1990s were marked by a regain of interest for that type of spillway design. Most structures had flat horizontal steps, but some were equipped with devices to enhance energy dissipation. Some spillways had pooled steps with vertical walls or inclined upward steps. Enhancement of energy dissipation may be provided by superposition of small and large steps, incorporation of occasional large steps to smaller steps, or V-shaped step edges (review by Chanson and Gonzalez 2004).
There is some analogy between skimming flows over stepped chutes and skimming flows above large roughness elements, including boundary layer flows past d-type roughness. Djenidi et al. (1999) provided a comprehensive review of the latter, while Aivazian (1996) studied zigzag strip roughness. Mochizuki and co-workers (1993,1996) studied turbulent

boundary layer past d-type roughness with thin longitudinal ribs. Despite conflicting interpretations of their data, their experiments demonstrated some turbulence manipulation by interfering with the recirculation vortices.

Fig. 1 - Experimental facility
(a) Air-water flow down the stepped chute next to the inception point of free-surface aeration - Flow from left to right note the strong deformation of the free-surface - Configuration 3 with 7 vanes in line ($d_c/h = 1.7$)

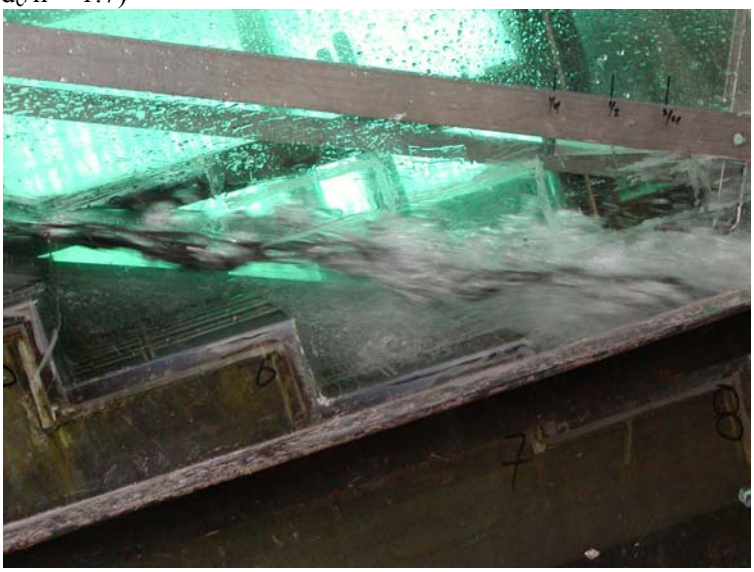

(b) Spray and droplet generation captured with high-shutter speed - Flow from left to right - Configuration 2 with 3 vanes in line ($d_c/h = 1.1$)

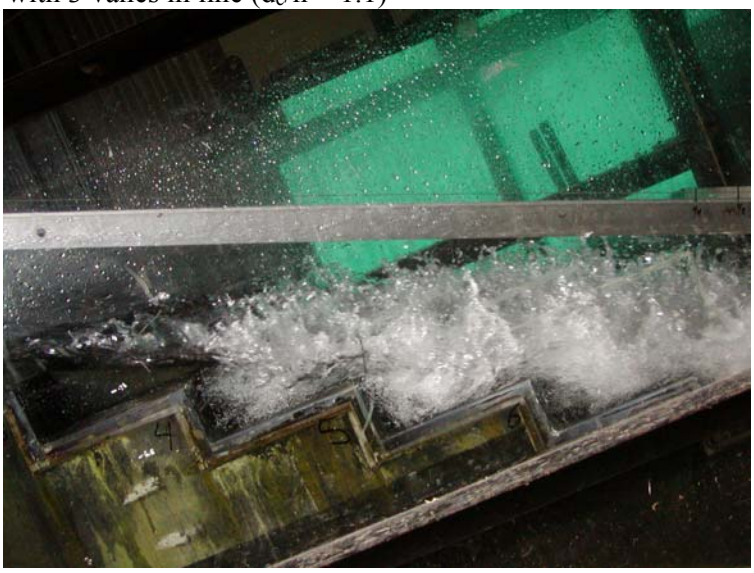

2. Experimental setup

New experiments were conducted at the University of Queensland in a 3.3 m long, 1 m wide, 21.8º slope chute previously used by Chanson and Toombes (2002). Waters were supplied from a large feeding basin (1.5 m deep, surface area 6.8 m×4.8 m) leading to a sidewall convergent with a 4.8:1 contraction ratio. The test section consisted of a broad-crested weir (1 m wide, 0.6 m long, with upstream rounded corner (0.057 m radius)) followed by ten identical steps (h = 0.1 m, l = 0.25 m) made of marine ply. The stepped chute was 1 m wide with perspex sidewalls followed by a horizontal concrete-invert canal ending in a

dissipation pit. For three series of experiments, the step cavity were equipped with vanes or longitudinal thin ribs (Fig. 2, Table 1).

A pump controlled with an adjustable frequency AC motor drive delivered the flow rate, enabling an accurate discharge adjustment in a closed-circuit system. Clear-water flow depths were measured with a point gauge. Air-water flow properties were measured using a double-tip conductivity probe (∅ = 0.025 mm) designed at the University of Queensland. The probe sensors were aligned in the flow direction. The leading tip had a small frontal area (i.e. 0.05 mm^2) and the trailing tip was offset to avoid wake disturbance from the first tip. Tests showed the absence of wake disturbance during all experiments (Chanson 1995). An air bubble detector (UQ82.518) excited the probe and its output signal was scanned at 20 kHz for 20 seconds. The translation of the probes in the direction normal to the channel invert was controlled by a fine adjustment traveling mechanism connected to a Mitutoyo™ digimatic scale unit (Ref. No. 572-503). The error on the vertical position of the probe was less than 0.025 mm. The accuracy on the longitudinal probe position was estimated as $\Delta x < +/- 0.5$ cm. The accuracy on the transverse position of the probe was less than 1 mm. Flow visualisations were conducted with high-shutter speed digital still- and video-cameras.

Fig. 2 - Sketch of turbulence manipulators (vanes) inserted in step corners

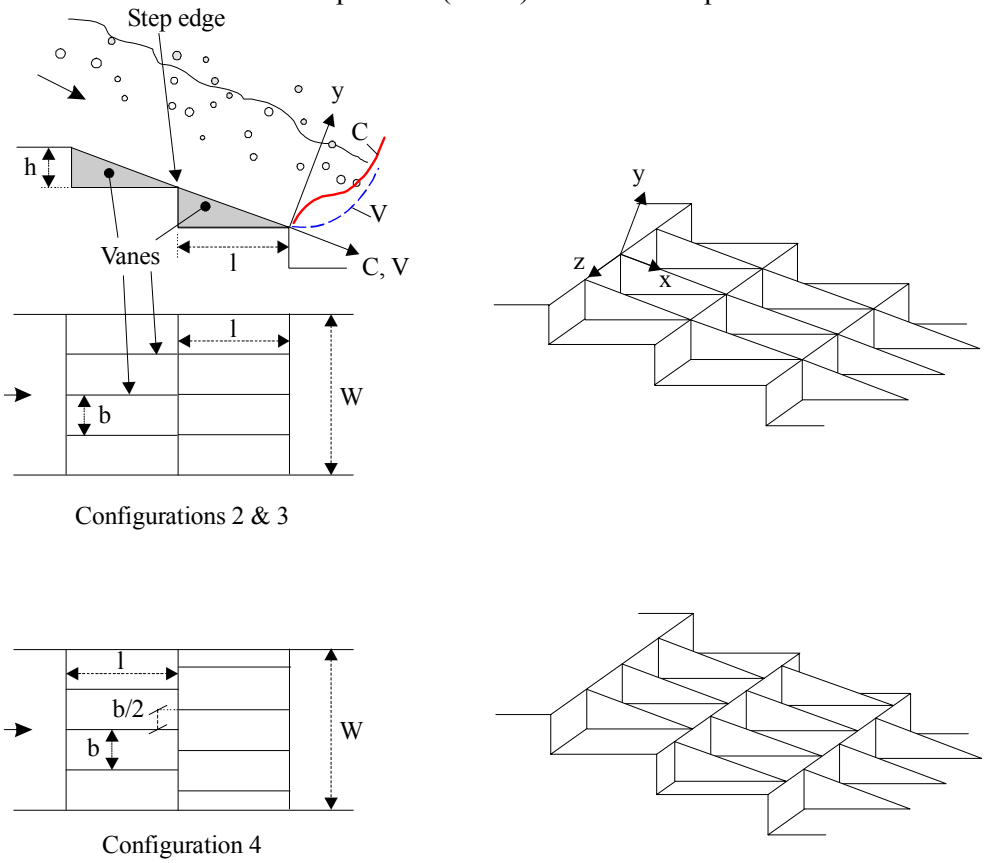

Configurations 2 & 3

Configuration 4

Data processing

The basic probe outputs were the void fraction, bubble count rate, velocity, turbulence intensity and air/water chord size distributions (e.g. Crowe et al. 1998, Chanson 2002). The void fraction C is the proportion of time that the probe tip is in the air. The bubble count rate F is the number of bubbles impacting the probe tip. The bubble chord times provide information on the air-water flow structure. With a dual-tip probe design, the velocity measurement is based upon the successive detection of air-water interfaces by two tips. In turbulent air-water flows, the detection of all bubbles by each tip is highly improbable and it

is common to use a cross-correlation technique (e.g. Crowe et al. 1998). The time-averaged air-water velocity equals : $V = \Delta x / T$, where Δx is the distance between tips and T is the time for which the cross-correlation function is maximum. The turbulent intensity Tu = u'/V may be derived from the broadening of the cross-correlation function compared to the auto-correlation function (Chanson and Toombes 2002):

$$Tu = 0.851 * \frac{\sqrt{\Delta T^2 - \Delta t^2}}{T} \quad (2)$$

where ΔT as a time scale satisfying : $R_{xy}(T+\Delta T) = 0.5*R_{xy}(T)$, R_{xy} is the normalized cross-correlation function, and Δt is the characteristic time for which the normalized autocorrelation function R_{xx} equals 0.5.

Chord sizes may be calculated from the raw probe signal outputs. The results provide a complete characterization of the streamwise distribution of air and water chords. In turn information on the flow structure may be analyzed in terms of particle clustering and grouping (Chanson and Toombes 2002). In this study, two air bubbles are parts of a cluster when the water chord separating the bubbles is less than one tenth of the mean water chord size. The measurement of air-water interface area is a function of void fraction, velocity, and bubble sizes. For any bubble shape, bubble size distribution and chord length distribution, the specific air-water interface area a defined as the air-water interface area per unit volume of air and water may be derived from continuity: a = 4*F/V.

Table 1 - Detailed experimental investigations of air entrainment on moderate slope stepped chutes

Reference	θ deg.	q_W m^2/s	h m	Re	Instrumentation	Remarks
(1)	(2)	(3)	(4)	(5)	(6)	(7)
Chanson and Toombes (2002)	21.8	0.06 to 0.18	0.1	2.4E+5 to 7.2E+5	Double-tip conductivity probe (∅ = 0.025 mm)	L = 3.0 m. W = 1 m. Inflow: uncontrolled broad-crest. Experiments TC200.
	15.9	0.07 to 0.19	0.1	2.8E+5 to 7.6E+5	Double-tip conductivity probe (∅ = 0.025 mm)	L = 4.2 m. W = 1 m. Inflow: uncontrolled broad-crest. Experiments TC201.
Gonzalez and Chanson (2004)	15.9	0.020 to 0.200	0.05	8E+4 to 8E+5	Double-tip conductivity probe (∅ = 0.025 mm)	L = 4.2 m. W = 1 m. Inflow: uncontrolled broad-crest. Experiments CG202.
		0.075 to 0.220	0.10	3E+5 to 8.7E+5		Incl. detailed measurements between step edges.
Present study Configuration 1 Configuration 2 Configuration 3 Configuration 4	21.8	0.10 to 0.22	0.1	4E+5 to 8.7E+5	Double-tip conductivity probe (∅ = 0.025 mm)	L = 3.3 m. W = 1 m. Inflow: uncontrolled broad-crest. Experiments CG203. b = W = 1 m (no vane). b = W/4 = 0.25 m (3 vanes in line). b = W/8 = 0.125 m (7 vanes in line). b = W/8 = 0.125 m (7 vanes in zigzag).

Notes : L : chute length; W : chute width.

Spectral analysis

The autocorrelation function provides some information on the air-water flow structure. A Fourier spectral analysis gives further information on the frequency distribution of the signal that is related to the air+water (& water+air) length scale distribution of the flow (Fig. 3).

The signal outputs from the dual-tip probe are binary signals recorded simultaneously.

Considering the bubble striking at the probe as a stochastic process, the leading tip signal auto power spectrum may provide some information on stationarity and periodicity, and show specific features of the air-water flows structure. In a typical auto power spectrum (Fig. 4), the vertical axis represents the energy density in (J/Hz) and the horizontal axis is the frequency in Hz. The power spectral density (PSD) curve displays the partitioning of power, or voltage variation (interface length scale fluctuation) according to frequency. The frequency of voltage fluctuation (f) is a function of the velocity at which the interfaces are convected past the probe (local flow velocity V) and on the air+water length scale that may be calculated as $\lambda = V/f$ (Fig. 3). A combined analysis of chord length, clustering and spectral characteristics describes the air-water flow structure and its behavior.
In the particular case of a stepped chute flow, a comparison between cavity flow and stream flow characteristics may provide new information on the basic hydrodynamic processes.

Fig.3 - Sketch of probe output signal and definition of air+water interface chord length

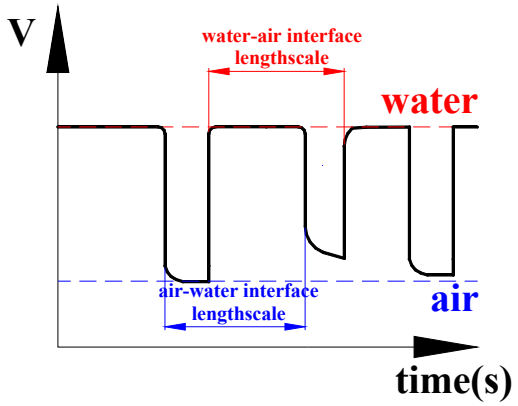

Fig.4 - Power spectral density obtained between step edges 9 &10, X = 0.2, y = -26mm (below pseudo-bottom) for $d_c/h = 1.5$ (Skimming Flow)

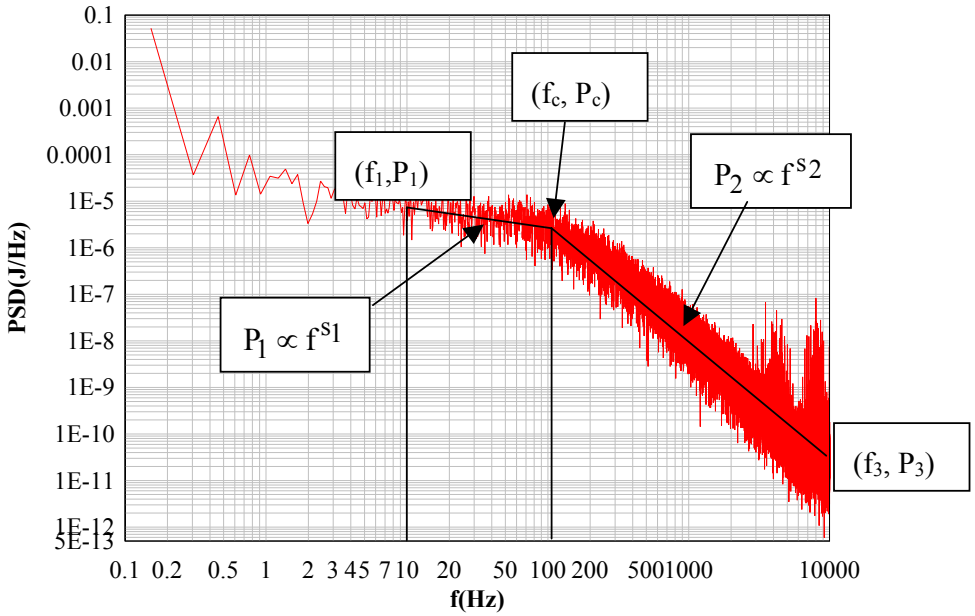

Discussion

Experimental observations highlighted the three-dimensional nature of recirculation vortices in step cavities beneath the pseudo-bottom formed by the step edges. In absence of vane (see

below), three to four cavity recirculation cells were observed across the channel width. The finding was consistent with similar observations by Drs. Matos and Yasuda (Pers. Comm.) on steeper slopes. These recirculation vortices are related to longitudinal (streamwise) coherent structures in the mainstream flow.
In the present study, four stepped geometries were tested systematically. The first had ten identical flat horizontal steps. In the second, third and fourth configurations, vanes or longitudinal ribs were placed across the step cavity from steps 2 to 10 as illustrated in Figure 2. The second and third configurations had 3 and 7 vanes in line respectively (Table 1). The fourth configurations had 7 vanes set in zigzag (Fig. 2). The vanes were made of aluminum but for few in perspex next to the sidewall for flow visualization. The vanes did not interfere with the free-stream.
Experimental observations were conducted for flow rates ranging from 0.10 to 0.22 m^3/s corresponding to a skimming flow regime (Table 1). Measurements were performed at step edges and between adjacent step edges (i.e. above recirculation cavity).

3. Basic results

3.1 Flow patterns

In skimming flows, the water free-surface was smooth and no air entrainment occurred at the upstream end of the cascade. After a few steps the flow was characterized by a strong air entrainment. Downstream, the two-phase flow behaved as a homogeneous mixture and the exact location of the interface became undetermined. There were continuous exchanges of air-water and of momentum between the main stream and the atmosphere, while intense cavity recirculation was observed. The mainstream air-water flow consisted of a bubbly flow region ($C < 30\%$), a spray region ($C > 70\%$) and an intermediate flow structure for $0.3 < C < 0.7$.
At the inception of free-surface aeration, the flow was rapidly varied (Fig. 1a). Side view observations suggested that some air was entrapped by a flapping mechanism in the step cavity(ies) immediately upstream of the visual location of free-surface aeration. In presence of vanes, aeration of two to three cavities were seen upstream of inception, while only one to two aerated cavities were observed in absence of vanes.
Flow visualizations next to the chute sidewall and near the inception point of free-surface aeration highlighted the effects of vanes on cavity recirculation. Although the vanes did not interfere with the stream flow, they were subjected to strong transverse pressure forces: i.e., in the horizontal direction z normal to the stream flow direction. The pressure load fluctuations appeared to be of the same period and in phase with cavity fluid ejections described by Djenidi et al. (1999) for d-type roughness flow and Chanson et al. (2002) for stepped chute flows.
In configurations 2 and 3 (vanes in line), visual observations suggested the development of longitudinal troughs above the vanes, associated with some wake effect above each one.

3.2 Void fraction and velocity distributions

Detailed measurements of void fraction and air-water velocity were conducted downstream of the air entrainment inception point. For stepped configurations with vanes, measurements were conducted systematically at $z = 0$, $b/4$ and $b/2$, where z is the transverse direction with $z = 0$ on the channel centerline above a series of vanes and b is the spacing between vanes (Fig. 2).
For all stepped configurations, air concentration distributions highlighted smooth profiles that followed closely an analytical solution of the bubble advective diffusion equation for $y > 0$ where y is the distance normal to the pseudo-bottom formed by the step edges (Chanson and Toombes 2002). Between step edges, strong aeration was recorded in the step cavities (i.e. $y < 0$). The results showed little effects of the vanes on the void fraction results, but immediately above the vanes ($z = 0$, configurations 2 and 3).
Velocity measurements demonstrated however that the effect of the vanes was not limited to

the cavity flow but extended into the main stream. The velocity distributions showed some marked difference in presence of vanes for $y/Y_{90} < 0.6$ to 0.7 at all transverse positions (z/b = 0, 0.25 & 0.5). Velocity measurements between step edges highlighted further a developing mixing layer downstream of each step edge and best seen for $-0.3 < y/Y_{90} < +0.2$ (Gonzalez and Chanson 2004). These trends are illustrated in Figures 5 and 7 at step edge and Figures 6 and 8 between step edges.

Figure 5a presents typical dimensionless distributions of air concentration C and velocity V/V_{90} at step edge, where V_{90} is the characteristic velocity at $y = Y_{90}$, and Y_{90} is the distance where C = 0.90. In Figure 5a, the depth-averaged void fraction C_{mean} equals 0.36 (no vane), 0.33 (3 vanes, $z/b = 0$) and 0.37 (3 vanes, $z/b = 0.5$) where C_{mean} is defined as:

$$C_{mean} = \frac{1}{Y_{90}} \int_0^{Y_{90}} C \, dy \tag{1}$$

Figure 5b shows dimensionless distributions of bubble frequency F^*d_c/V_c and turbulence intensity Tu at step edge, where F is the bubble count rate, d_c the critical flow depth, and V_c is the critical velocity. In Figure 6, air-water flow properties between step edges are presented. Figure 6a shows typical dimensionless distributions of air concentration C and velocity V/V_{90} while Figure 6b presents turbulence intensity Tu and bubble frequency F^*d_c/V_c data. All data were obtained between step edges at X = 0.25, where $X = x/L_{cav}$, L_{cav} is the cavity length and x is the streamwise distance from the upper step corner, with X = 0 and 1 at the upstream and downstream step edges respectively. Data for $y < 0$ were recorded in the step cavity.

Figure 7a presents a comparison of air concentration C and velocity V/V_{90} distributions obtained at step edge between Configurations 3 (7 vanes in line) and 4 (7 vanes in zigzag). Fig. 7b shows bubble frequency F^*d_c/V_c and turbulence intensity Tu distributions obtained at step edge. Figure 8a shows air concentration and velocity distributions between step edges at X = 0.25 for Configurations 3 and 4. Figure 8b presents bubble frequency F^*d_c/V_c and turbulence intensity Tu distributions for the same conditions (obtained between step edges at X = 0.25 for configurations 3 and 4).

Discussion

Present velocity observations showed a low-velocity region for $y/Y_{90} < 0.5$ above the vanes ($z/b = 0$) which is consistent with a wake region. Holmes et al (1996) proposed the existence of pairs of counter-rotating streamwise vortices or "rolls" next to the wall in turbulent boundary layers, associated with a region of reduced velocity in the stream direction. Above vanes, quasi-coherent wakes, somehow similar to low-speed streaks, were seen interfering with the main stream. Such turbulent structures were best observed next to the inception point of free-surface aeration, but are believed to occur further downstream.

It is believed that the effects of the vanes onto the main flow were two-fold. Firstly the presence of vanes prevented the spanwise development of large coherent structures in the step cavities ($y < 0$). Secondly they led to the appearance of longitudinal (streamwise) coherent "wake" structures in the mainstream flow ($y > 0$). Such coherent structures affects momentum exchange between cavity and stream flows, and hence the rate of energy dissipation.

Overall the observed results suggested that the vanes strongly influenced the flow in both the cavities below the pseudo-bottom formed by the step edges and the main stream.

Fig. 5 – Comparison between Configuration 1 (no vane) and Configuration 2 (3 vanes, z/b = 0 & 0.5) at step edge (d_c/h = 1.5). (a) Dimensionless distributions of air concentration and velocity at step edge 9. (b) Dimensionless distributions of bubble frequency and turbulence intensity at same location.

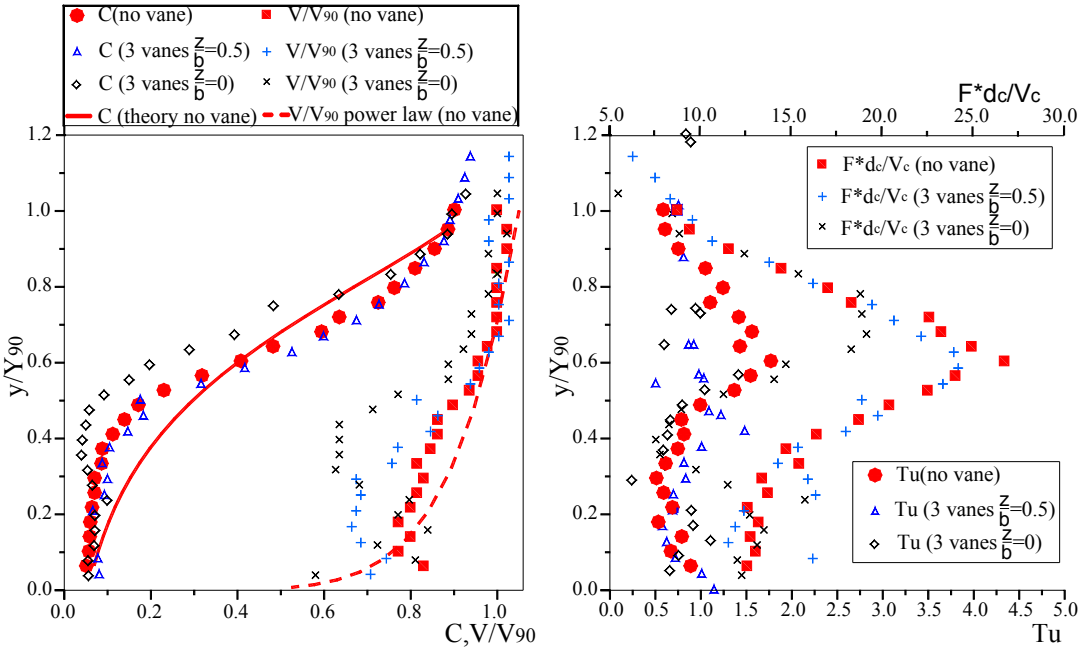

(a) (b)

Fig. 6 – Comparison between Configuration 1 (no vane) and Configuration 2 (3 vanes, z/b = 0 & 0.5) between step edges (d_c/h = 1.5). (a) Dimensionless distributions of void fraction and velocity at 25% of the distance between step edges 9 and 10 (X = 0.25). (b) Dimensionless distributions of bubble frequency and turbulence intensity at same location.

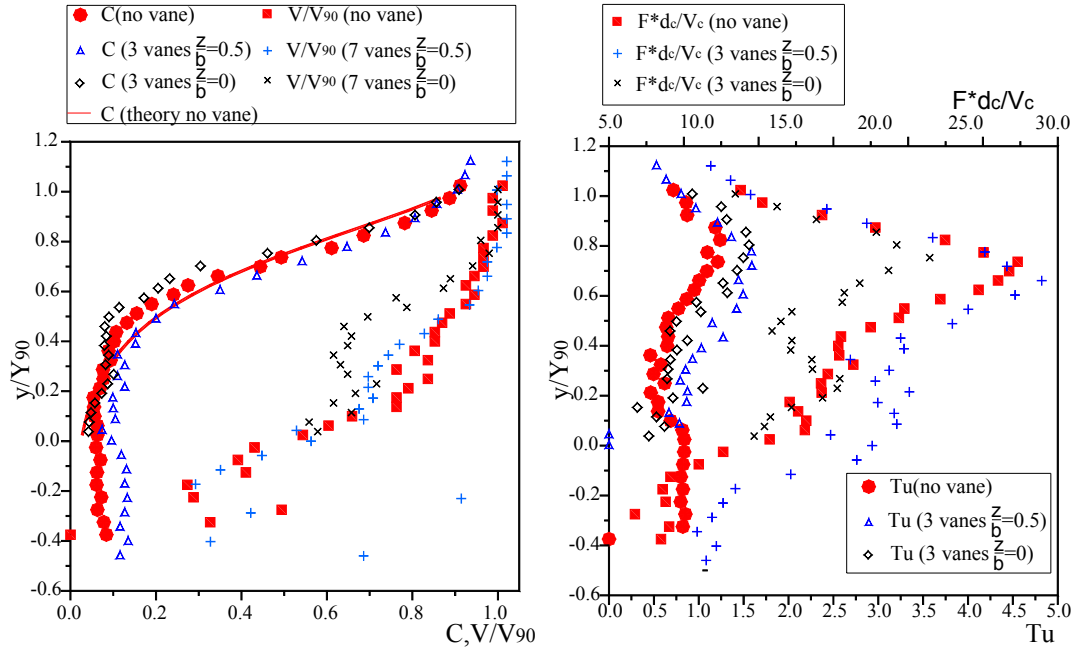

(a) (b)

Fig. 7 – Comparison between Configuration 3 (7 vanes in line) and Configuration 4 (7 vanes in zigzag, z/b = 0 & 0.5) (d_c/h = 1.5). (a) Dimensionless distributions of air concentration and velocity at step edge 9. (b) Dimensionless distributions of bubble frequency and turbulence intensity at same location.

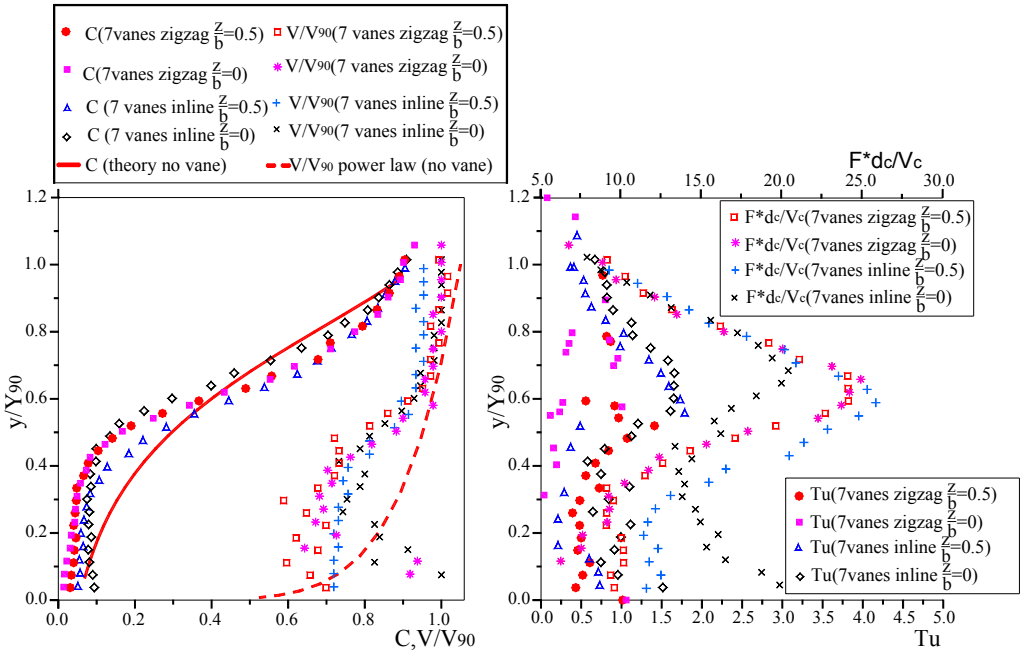

Fig. 8 – Comparison between Configuration 3 (7 vanes in line) and Configuration 4 (7 vanes in zigzag, z/b = 0 & 0.5) (d_c/h = 1.5). (a) Dimensionless distributions of void fraction and velocity at 25% of the distance between step edges 9 and 10. (b) Dimensionless distributions of bubble frequency and turbulence intensity at same location.

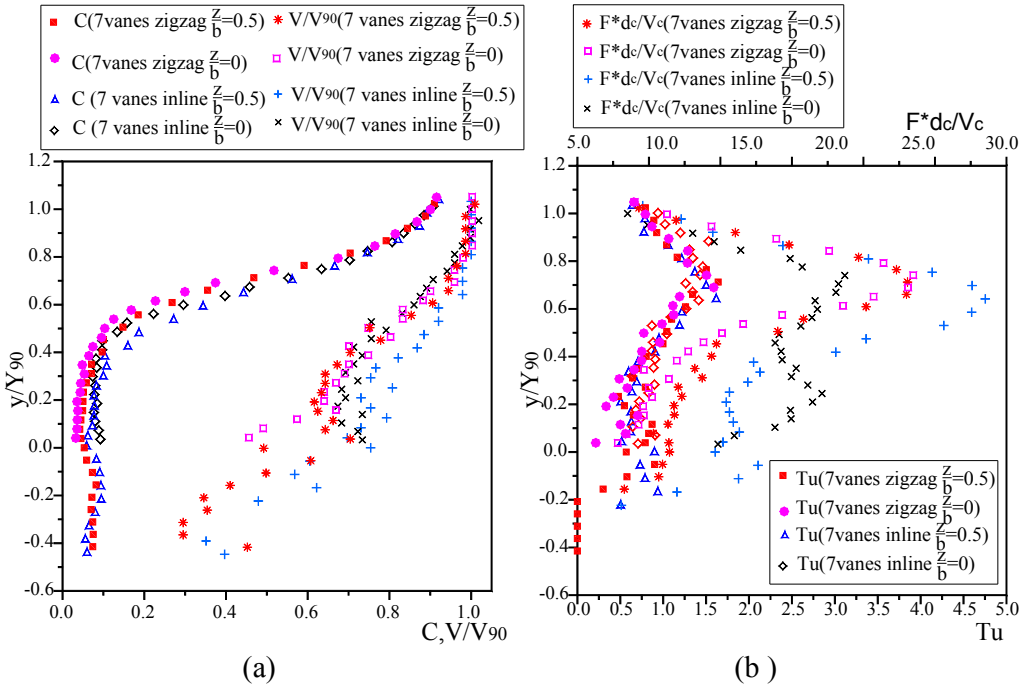

Flow resistance and mechanisms of energy dissipation

The rate of energy dissipation and hence the flow resistance were deduced from the average

friction slope (e.g. Chanson et al. 2002). For stepped configurations with vanes, the flow resistance was calculated at z/b = 0 (above vane), z/b = 0.25 and z/b = 0.5. In average the experimental results implied equivalent Darcy friction factors of about 0.26, 0.32, 0.29 and 0.35 for configurations 1, 2, 3 and 4 respectively. Basically they suggested that the presence of vanes increased the flow resistance, and the largest rate of energy dissipation was achieved with 7 vanes in zigzag.

It is believed that the vanes prevented the development of transverse turbulence in the cavities. The inhibition of large transverse vortical structures was associated with enhanced vertical mixing between recirculation zones and mainstream that was characterized by irregular fluid ejections, turbulent bursts and sweeps. Turbulent mixing enhancement in turn yielded greater spray generation. If the water mass flux in the "mist" region is defined as :

$$q_{mist} = \int_{Y_{90}}^{Y_{99}} (1 - C) * V * dy \qquad (2)$$

where Y_{99} is the distance where C = 0.99, experimental results showed consistently that the dimensionless water flux in the mist q_{mist}/q_w was about 5-10% in absence of vanes (configuration 1), and increased to about 20-30% for configurations 2, 3 and 4 (with vanes). The largest mist flux was observed for Configuration 2 although there was little difference between Configurations 2, 3 and 4.

4. Air-water flow structure

4.1 Air-water interface chord length

With an intrusive phase-detection probe, the flow maybe analysed in terms of streamwise air or water structures bounded by air-water interfaces detected by the probe sensor (Fig. 3). Bubbly turbulent flows do not contain single-size bubbles, but a broad range of air-bubbles and water chords with different sizes.

In Figure 9, typical probability distribution functions (PDF) of bubble chord sizes are presented for measurements corresponding to Configurations 1 to 4 obtained below the pseudo-bottom (y < 0) and between vanes (z/b = 0.5). For all configurations, the predominant air-bubble chord length was between 0.5 and 1.0 mm, and the distributions were skewed with a preponderance of bubbles smaller than the mean. Figure 10 presents PDF of air-bubble chord sizes for measurements made in similar conditions and with similar air concentrations as in Figure 9, but above the pseudo-bottom. In Figure 11, PDF of water-droplet chord sizes measured in the spray region (C > 0.9) are presented.

For all configurations, the predominant air-bubble chord length in bubbly flow region (C < 0.3) is between 0.5 and 1.5 mm. It is worth noting the differences between Fig. 9 and Fig. 10, where the amount of bubbles detected in the mainstream (Fig. 10) were at least twice as much as that detected in the cavity recirculation region (y < 0), for the same void fraction and data logging time. Although the histogram mode (predominant bubble size) was 0.5 mm at both locations (i.e. y< 0 & y > 0), bubble chord distributions at locations below pseudo-bottom (Fig. 9) were less skewed than those within the mainstream (Fig. 10), implying larger bubbles in average in the recirculation region.

The predominant size of water-droplets in the spray region was 0.5 mm, but a wide range of droplet sizes was observed : e.g., 75% of water droplets had sizes varying from 1 to 8.5 mm in Figure 11.

Fig.9 Air-bubble chord-length distribution histograms. d_c/h = 1.5 Configurations 1 to 4 between step edges 9 and 10 at X = 0.25, below pseudo-bottom (y < 0) and z/b = 0.5

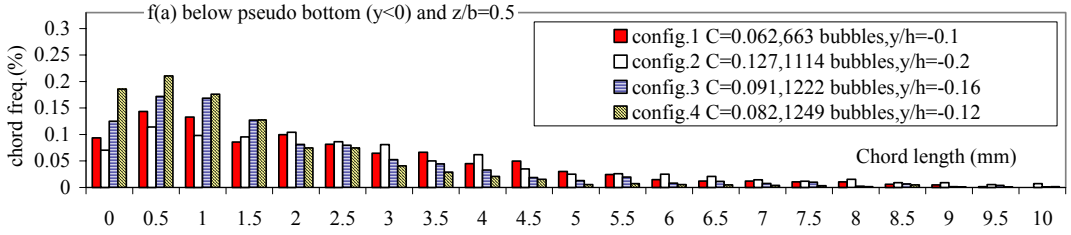

Fig.10 Air-bubble chord-length distribution histograms. d_c/h = 1.5 Configurations 1 to 4 between step edges 9 and 10 at X = 0.25, above pseudo-bottom (y > 0) and z/b = 0.5

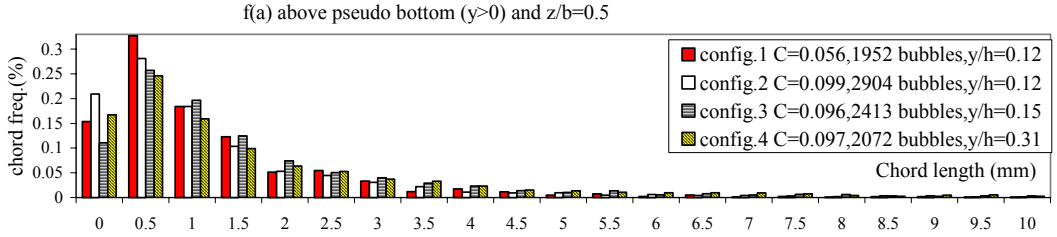

Fig.11 Water droplet chord-length distribution histograms. d_c/h = 1.5 Configurations 1 to 4 between step edges 9 and 10 at X = 0.25, spray region (C > 0.9) and z/b = 0.5

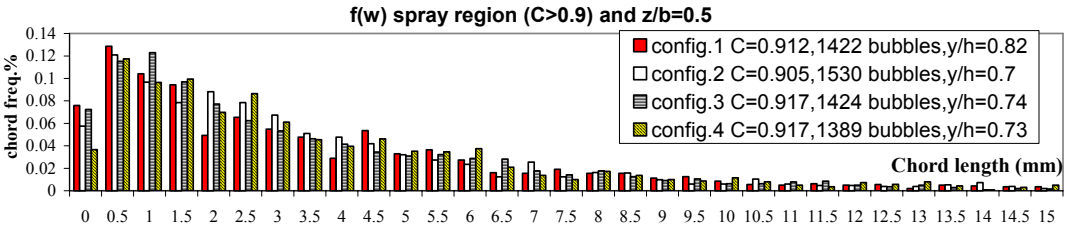

4.2 Clustering analysis

Air-bubbles and water-droplets clustering analyses were performed at different flow locations in both bubbly flow and spray regions. Typical results are shown in Figure 12, in terms of the probability distribution function (PDF) of number of bubbles per cluster for measurements in bubbly flow (C < 0.3) below (y < 0) and above (y > 0) the pseudo-bottom for all configurations. Data obtained at locations below the pseudo-bottom showed similar tendencies, averaging approximately 15% of all bubbles were clustered and about 70% of clusters comprised two bubbles (Fig. 12a). Measurements made above the pseudo-bottom showed nearly identical results (Fig. 12b).

In the spray region (C > 0.9) only 5% of water droplets were clustered and 85% of those clusters comprised two droplets (Fig. 12c). The finding is consistent with the broad spectrum of water droplet size (Fig. 11)

Overall, the cluster analysis results showed a significant proportion of air-bubbles clustered mainly in 2 particle structures (along the streamwise direction). This is in agreement with previous observations by Chanson and Toombes (2002).

Further visual observations showed that cavity fluid ejection took place, at irregular time intervals, primarily at the downstream of the cavity. Air/water chord length and clustering analyses were performed for different streamwise locations along the cavity (i.e. X = 0.25, 0.5 & 0.75). Despite recirculating eddy presence and mixing layer influence, results showed that

the flow structure (air-bubble and water droplet clusters) did not vary much with its stream wise position X (i.e. along cavity length).

Fig.12 Air bubbles and water droplets clustering in bubbly and spray flow for configurations 1 to 4.

(a) below pseudo-bottom (y < 0) and z/b = 0.5

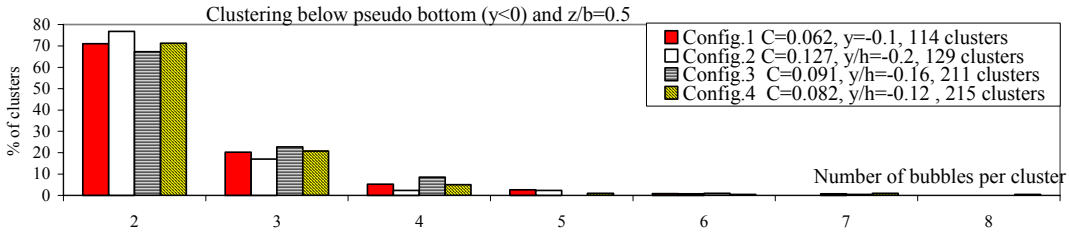

(b) above pseudo-bottom (y < 0) and z/b = 0.5

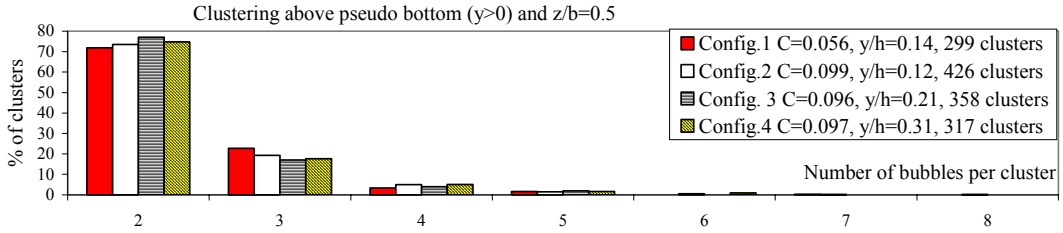

(c) water droplet clustering in spray region (C > 0.9) and z/b = 0.5.

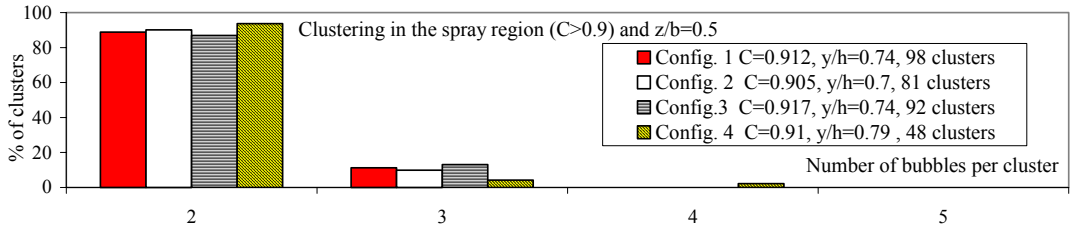

4.3 Spectral analysis

For one cavity in configuration 1 (no vane), a spectral analysis was conducted systematically for several locations at step edges and above the cavity : X = 0.25, 0.5 and 0.75. A typical result is shown in Figure 4. Figure 4 presents a typical power spectrum distribution (PSD) data curve at a location between step edges (X = 0.2) and below pseudo-bottom (y < 0). Disregarding the lowest frequency range, the spectrum can be roughly divided in two zones, corresponding to two straight lines with different slope s_1 and s_2. Each straight lines represent the power functions in the linear scale with the value of the slopes as exponents of the functions $P_1 \propto f^{s1}$ and $P_2 \propto f^{s2}$, where P represents the value of the PSD in (J/Hz) and f is the frequency in Hz.

Zone 1 represents the total energy in the signal due to the largest length scales, while Zone 2 corresponds to the total energy of the signal for the smaller scales. No peak corresponding to a dominant frequency was observed, but a characteristic frequency corresponding to the change of slope (f_c) was noticed consistently (Fig. 4). The physical meaning of such spectrum shape is still unknown, but f_c is expected to provide a some information on the signal periodicity and associated air+water length scales. For a typical observation f_c = 100 Hz and V

= 1.2 m/s (Fig. 4), the characteristic length scale is λ_c = 6 mm. Lastly the area under the total spectrum curve represents the Total Energy (T_E) contained in the signal

The most remarkable results obtained from the spectral analysis are the followings. (1) The value of the slope s_1 (Zone 1) showed different values at different depths y, with low values ($s_1 \sim -0.8$) for measurements in the bubbly zone ($C < 0.3$), larger values ($s_1 \sim -1.3$) in the intermediate zone ($0.3 < C < 0.7$) and moderate values ($s_1 \sim -0.9$) in the spray region($C > 0.7$). This finding suggests that the grouping of air+water structures with a length scale larger than λ_c vary with depth, void fraction and bubble count rate. (2) On the other hand, the value of the slope s_2 (Zone 2) was nearly constant ($s_2 \sim -2.6$) through all vertical profiles at all locations. The result might suggest that interfaces with length scales smaller than the characteristic scale $\lambda_c = V/f_c$ were roughly independent of, or insensitive to, the turbulent flow conditions and air-water flow properties. (3) The characteristic length scale λ_c was typically about 10 mm : i.e., $5 < \lambda_c < 17$ mm. (4) Finally, it was observed that the values of total energy (T_E) were similar for different locations with similar void fractions. This was expected.

In turbulent flow literature (Tennekes and Lumley 1972, Hinze 1975, Pope 2000), the turbulent energy spectrum is usually divided into three zones. Zone A or "Energy containing range" is the lowest frequency region, Zone B or Inertial sub range is the intermediate part of the spectrum, and Zone C or dissipation range is the largest frequency part of the spectra. In the present study the same division does not apply because the basic signal is voltage (or conductivity) rather than velocity, but the overall shape is somehow similar to the shape of turbulent energy spectrum.

Conclusion

Interactions between free-surface and cavity recirculation, as well as turbulence manipulation were systematically investigated in the skimming flow regime down a stepped chute, in a large-size facility at large Reynolds numbers (Table 1). Four stepped geometries were studied The first had ten identical flat horizontal steps. In the second, third and fourth configurations, vanes or longitudinal ribs were placed across the step cavity to block the development of three-dimensional recirculation cells in the step cavity, while they did not intrude into the free-stream skimming flow (Fig. 2).

Basic results demonstrated a strong influence of the vanes on the air-water flow properties of both free-stream and cavity flows. The overall rate of energy dissipation was affected by the step configuration, and maximum form drag was observed with a stepped configuration with 7 vanes in zigzag (Configuration 4). The presence of vanes was twofold. The vanes prevented the spanwise development of cavity recirculating eddies, while they contributed to the development of a wake region above each vane. Further the air-water flow structure (bubble/droplet size distributions, clusters) was affected by the presence of vanes. This was possibly best seen in the bubbly flow region of the mainstream flow (Fig. 10). A spectral analysis of the probe signal output was conducted. Preliminary results suggested that small air+water structures, with length scales smaller than a characteristic scale λ_c, were little affected by the air-water turbulent flow conditions.

Overall the study provides new information on the complex interactions between turbulence and flow aeration in flows with large Reynolds numbers. The results show further that turbulence manipulation is achievable, and that the technique is applicable to stepped spillway to enhance the rate of energy dissipation.

Acknowledgements

The writers thank Mr G. Illidge for his assistance and Professor C.J. Apelt his valuable advice. The second writer acknowledges the financial support of the National Council for Science and Technology of Mexico (CONACYT) and of the University of Queensland.

References

Aivazian, O.M. (1996). "New Investigations and new Method of Hydraulic Calculation of Chutes with Intensified Roughness." *Gidrotekhnicheskoe Stroitel'stvo*, No. 6, pp. 27-39 (in Russian). (Translated in Hydrotechnical Construction, 1996, Plenum Publ., Vol. 30, No. 6, pp. 335-356.)

Chanson, H. (1995). "Air Bubble Entrainment in Free-surface Turbulent Flows. Experimental Investigations." *Report CH46/95*, Dept. of Civil Engineering, University of Queensland, Australia, June, 368 pages.

Chanson, H. (1997). "Air Bubble Entrainment in Free-Surface Turbulent Shear Flows." *Academic Press*, London, UK, 401 pages. {http://www.uq.edu.au/~e2hchans/reprints/book2.htm}

Chanson, H. (2001). "The Hydraulics of Stepped Chutes and Spillways." *Balkema*, Lisse, The Netherlands, 418 pages. {http://www.uq.edu.au/~e2hchans/reprints/book4.htm}

Chanson, H. (2002). "Air-Water Flow Measurements with Intrusive Phase-Detection Probes. Can we Improve their Interpretation ?." *Jl of Hyd. Engrg.*, ASCE, Vol. 128, No. 3, pp. 252-255.

Chanson, H., and Gonzalez, C.A. (2004). "Stepped Spillways for Embankment dams: Review, Progress and Development in Overflow Hydraulics." *Proc. Intl Conf. on Hydraulics of Dams and River Structures*, Tehran, Iran, Balkema Publ., The Netherlands, 8 pages (in Print).

Chanson, H., and Toombes, L. (2002). "Air-Water Flows down Stepped Chutes: Turbulence and Flow Structure Observations." *Intl Jl of Multiphase Flow*, Vol. 27, No. 11, pp. 1737-1761 (ISSN 0301-9322).

Chanson, H., Yasuda, Y., and Ohtsu, I. (2002). "Flow Resistance in Skimming Flows and its Modelling." *Can Jl of Civ. Eng.*, Vol. 29, No. 6, pp. 809-819 (ISSN 0315-1468).

Crowe, C., Sommerfield, M., and Tsuji, Y. (1998). "Multiphase Flows with Droplets and Particles." *CRC Press*, Boca Raton, USA, 471 pages.

Djenidi, L., Elavarasan, R., and Antonia, R.A. (1999). "The Turbulent Boundary Layer over Transverse Square Cavities." *Jl Fluid Mech.*, Vol. 395, pp. 271-294.

Gonzalez, C.A., and Chanson, H. (2004). "Interactions between Cavity Flow and Main Stream Skimming Flows: an Experimental Study." *Can Jl of Civ. Eng.*, Vol. 31 (In Print).

Hinze, J. O. (1975). "Turbulence", *McGraw-Hill*, New York.

Holmes, P., Lumley, J.L., and Berkooz, G. (1996)."Turbulence, Coherent Structures, Dynamical Systems and Symmetry." *Cambridge University Press*, Cambridge, UK,pp.63-77

Mochizuki, S., and Osaka, H. (1993). "Two-Point Velocity Correlation Measurement in a d-type Rough Wall Boundary Layer Modified with the Longitudinal Thin Ribs." *Proc. 9th Symp. on Turbulent Shear Flows*, Kyoto, Japan, Aug. 16-18, paper 5-2, 6 pages.

Mochizuki, S., Izawa, A., and Osaka, H. (1996). "Turbulent Drag Reduction in a d-type Rough Wall Boundary Layer with Longitudinal Thin Ribs Placed within Traverse Grooves (Higher-order Moments and Conditional Sampling Analysis)." *Trans. JSME Intl Journal*, series B, Vol. 39, No. 3, pp. 461-469.

Pope, S. B. (2000). "Turbulent Flows", *Cambridge University Press*, Cambridge; New York.

Tennekes, H., and Lumley, J. L. (1972). "A first course in turbulence", *MIT Press*, Cambridge Mass., USA

Wood, I.R. (1991). "Air Entrainment in Free-Surface Flows." *IAHR Hydraulic Structures Design Manual No. 4*, Hydraulic Design Considerations, Balkema Publ., Rotterdam, The Netherlands, 149 pages.